

Direct determination of optimal real-space orbitals for correlated electronic structure of molecules.

Edward F. Valeev,^{*,†} Robert J. Harrison,[‡] Adam A. Holmes,[†] Charles C. Peterson,[¶] and Deborah A. Penchoff[§]

[†]*Department of Chemistry, Virginia Tech, Blacksburg, VA 24061*

[‡]*Department of Applied Mathematics & Statistics, Stony Brook University, Stony Brook, NY 11794*

[¶]*Office of Advanced Research Computing, University of California, Los Angeles, CA 90095*

[§]*UT Innovative Computing Laboratory, University of Tennessee, Knoxville, TN 37996*

E-mail: efv@vt.edu

September 14, 2023

Abstract

We demonstrate how to determine numerically nearly exact orthonormal orbitals that are optimal for evaluation of the energy of arbitrary (correlated) states of atoms and molecules by minimization of the energy Lagrangian. Orbitals are expressed in real space using a multiresolution spectral element basis that is refined adaptively to achieve the user-specified target precision while avoiding the ill-conditioning issues that plague AO basis set expansions traditionally used for correlated models of molecular electronic structure. For light atoms, the orbital solver, in conjunction with a variational electronic structure model [selected Configuration Interaction(CI)] provides energies of

comparable precision to a state-of-the-art atomic CI solver. The computed electronic energies of atoms and molecules are significantly more accurate than the counterparts obtained with the Gaussian AO bases of the same rank, and can be determined even when linear dependence issues preclude the use of the AO bases. It is feasible to optimize more than 100 fully-correlated numerical orbitals on a single computer node, and significant room exists for additional improvement. These findings suggest that the real-space orbital representations might be the preferred alternative to AO representations for high-end models of correlated electronic states of molecules and materials.

1 Introduction

Predictive computation of properties of molecules and materials requires highly-*accurate* treatment of many-electron correlation effects as well as *precise* numerical representation of the many-body states and operators involved therein. In molecular and, increasingly, in solid-state contexts many-body methods have utilized the Linear Combination of Atomic Orbitals (LCAO)¹ numerical representation of 1-particle (orbital) states constructed from pre-optimized sequences of atom-centered basis sets (represented by analytic Gaussian-type² or Slater-type functions,^{3,4} or represented numerically⁵). However, (augmented) plane-wave (PW) representation of 1-particle states can also be used.^{6,7} Unfortunately representation of many-particle by products of 1-particle states suffers from slow convergence in the vicinity of electron cusps,^{8,9} thereby mandating the use of basis set extrapolation¹⁰ or the augmentation with explicit 2-particle basis (“explicit correlation”).^{11–14}

Although the LCAO-based many-body methods can be pushed to match experimental thermochemical¹⁵ and spectroscopic data¹⁶ for small molecules, extending such successes to increasingly larger systems, and to higher accuracy, is limited by the rapid onset of ill-conditioning, high-order rise of operator evaluation with the AO angular momenta, and the challenges of fast (reduced-scaling) reformulation of such methods due to the increasing density of the representation in the high-precision regime. LCAO representation in practice is

a heavily empirical endeavour: at this moment the Basis Set Exchange reference database¹⁷ lists 402 Gaussian AO basis sets designed for representing orbitals of a carbon atom. Albeit the large number of officially-recognized bases is simply due to the long history of the Gaussian AO technology, many recently-designed bases have rather niche uses; navigating the basis set zoo is a near-expert task, especially when treating high-density solids^{18,19} or computing properties other than the energy.²⁰ Meanwhile plane wave representation struggles with description of localized features (e.g., atomic shell structure, nuclear cusps and Coulomb holes) of the electronic wave functions and thus are not naturally suitable to compact and/or fast formulations.

An attractive alternative to the LCAO and PW representations for many-body electronic structure are *real-space* numerical representations, a loosely-defined group including finite difference (FD), which only use grids and lack explicit basis functions, and finite element (FE) and spectral element (SE) methods, which utilize basis functions with strictly local support (i.e., the basis functions are only nonzero in a finite domain). Such representations combine the ability to resolve short and long lengthscale features of the many-body electronic wave functions with promise of systematic bias-free improvability without ill-conditioning issues. Due to these favorable features there has been a flurry of activity²¹⁻³⁰ in developing real-space numerical technology for fast 1-body methods, such as Kohn-Sham density functional theory.

Unfortunately the use of real-space representation has been far more limited for many-body methods applicable to general molecules due to the exponential growth of the representation of a k -particle state with k . Even methods like MP2 and CCSD in first-quantized formulation³¹ involve representation of 2-particle wave operators (hence, 6-dimensional functions); while for atoms pair theories have been explored for a relatively long time,³²⁻³⁵ for molecules the feasibility of such representations has been demonstrated only recently by some of us (MP2)^{36,37} and our collaborators (CIS(D), CC2)^{38,39} by combining volume-element-wise pair function compression and regularization of electron cusps³⁶ similar to that performed

in explicitly correlated R12/F12 methods.¹² It is possible to obtain energies and properties with such methods that are competitive to the state-of-the-art LCAO technology for small polyatomics, but the methodology is still relatively limited and likely cannot be made practical 3- and higher-body methods.

A more practical alternative to the direct real-space representation of 2-particle states is to expand them in products of real-space orbitals (also referred to as the algebraic approximation⁴⁰). Although such approaches, unlike the direct many-body representations, suffer from the slow convergence near electron cusps, the same remedies as used for the LCAO-based many-body methods (namely, the basis set extrapolation or R12/F12-style explicit correlation) can be deployed to fix these shortcomings. In the purely orbital-based many-body framework the key differences between spectral (LCAO, PW) and real-space representations is limited to the orbital optimization and evaluation of the physical operators. Due to the cost of both in the real-space representation, real-space many-body methods have been implemented for atoms (both at the multiconfiguration self-consistent field (MCSCF)^{41–43} and perturbative levels^{44,45}) and diatomic molecules (MCSCF,^{43,46,47} perturbation theory⁴⁸ and coupled-cluster (CC)^{49,50}); an excellent recent review of the vast relevant literature can be found in Ref. 51.

The first demonstration of any real-space orbital-based many-body method applicable to general molecules was shown recently by Kottmann, Bischoff, and Valeev.⁵² The key to this advance was the realization that far more compact orbital representation of the weakly-occupied (virtual) orbitals needed for dynamical correlation is provided by the pair-natural orbitals.^{53–55} The PNO-MP2-F12 method using the real-space representation for all orbitals was demonstrated for molecules with more than 30 atoms, with precision surpassing what is achievable by the state-of-the-art LCAO technology.

While the work showed a viable roadmap for developing many-body perturbation theory (MBPT) and related methods with real-space orbitals, a single Slater determinant often does not provide a qualitatively correct starting point. In this paper we ask whether it is possible

1. to express arbitrary (not just MBPT-based) orbital-based many-body wave functions in terms of real-space orbitals, and
2. robustly determine optimal design for such orbitals.

We conclude that the answer to these questions is affirmative.

Note that much the formalism for optimizing correlated real-space orbitals presented in this work is generic and can be used with any real-space representation. The specific numerical representation that we used here is based on the multiresolution analysis (MRA) of a Hilbert space that leads to adaptive construction of scale-invariant real-space discontinuous high-order spectral element bases.⁵⁶ The resulting multiresolution adaptive spectral element representation (or, simply, MRA representation)^{57–60} is usable for treating describing both valence and compact (core) electronic states with robust control of numerical error ϵ . The multiscale structure of the representation results in low-order computational complexity for treating large systems. A number of electronic structure methods have been demonstrated in the multiresolution representation, including one-body (Hartree-Fock and DFT²³) and 2-body (MP2,^{36,37} CC2³⁸) methods, with energies, forces, and other molecular properties^{39,61,62} of ground and excited states. The complete technical details of the numerical representation can be found in Refs.;^{23,59,63} for a pedagogical introduction the reader is referred to Ref. 64.

The rest of the paper is organized as follows. Section 2 describes the correlated multiresolution orbital solver. Section 3 describes the technical details of the computational experiments that are reported and analyzed in Section 4. Section 5 summarizes our findings and outlines future directions.

2 Formalism

Consider the energy functional of a (unit-normalized) state Ψ in a Fock-space state defined by M (spin-)orbitals $\{\phi_p\}$:

$$E(|\Psi\rangle) = \langle \Psi | \hat{H} | \Psi \rangle = \gamma_i^j h_j^i + \frac{1}{2} \gamma_{ij}^{kl} g_{kl}^{ij}, \quad (1)$$

where γ_j^i and γ_{kl}^{ij} are the (spin-orbital) 1- and 2-RDMs (see Appendix A for the notation and standard definitions). For a fixed *model* defining the map from orbitals $\{\phi_p\}$ to $|\Psi\rangle$, Eq. (1) defines a functional of the orbitals. Our objective is to minimize this functional with respect to M *orthonormal* orbitals $\{\phi_p\}$. Unlike the traditional representations of orbitals in terms of a fixed basis, such as an atomic orbital basis in the LCAO formalism, in this work each orbital is expressed in a basis *adaptively* refined to approach the orbital's exact representation in the full Hilbert space. The lack of a fixed basis precludes automatic enforcement of the orbital orthonormality by, e.g., unitary parametrization. Therefore it will be necessary to maintain orthonormality explicitly.

Here we follow the standard Lagrangian formalism for introducing orbital orthonormality constraints. Variation of the Lagrangian

$$L = \langle \Psi | \hat{H} | \Psi \rangle - \epsilon_j^i (s_j^j - \delta_i^j), \quad (2)$$

by replacement $\phi_m^* \rightarrow \phi_m^* + \delta$ produces the following first-order change:

$$\left\langle \frac{\partial L}{\partial \phi_m^*} \right\rangle = 2 \left(\gamma_i^m \hat{h} + \gamma_{ij}^{mk} \hat{g}_k^j - \epsilon_i^m \right) |\phi_i\rangle, \quad (3)$$

with \hat{g}_q^p defined in Eq. (28). The optimal orbitals are determined by solving

$$\left\langle \frac{\partial L}{\partial \phi_m^*} \right\rangle \stackrel{\text{opt}}{=} 0 \quad (4)$$

The multipliers are determined by projecting Eq. (4) onto the current (orthonormal) orbitals:

$$\left\langle \phi_n \left| \frac{\partial L}{\partial \phi_m^*} \right. \right\rangle = 2 (\gamma_i^m h_n^i + \gamma_{ij}^{mk} g_{nk}^{ij} - \epsilon_n^m) = 0, \quad \text{or} \quad (5)$$

$$\epsilon_n^m = \gamma_i^m h_n^i + \gamma_{ij}^{mk} g_{nk}^{ij}. \quad (6)$$

This choice of the multipliers makes the gradient automatically orthogonal to the current orbitals.

If $|\Psi\rangle$ is a single Slater determinant (SD) (e.g., a Hartree-Fock determinant) the RDMs simplify,

$$\gamma_j^i \stackrel{\text{SD}}{=} \delta_j^i, \quad (7)$$

$$\gamma_{kl}^{ij} \stackrel{\text{SD}}{=} \delta_k^i \delta_l^j - \delta_l^i \delta_k^j, \quad (8)$$

and the gradient becomes:

$$\left| \frac{\partial L}{\partial \phi_m^*} \right\rangle \stackrel{\text{SD}}{=} 2 \left(\hat{f} |\phi_m\rangle - f_i^m |\phi_i\rangle \right). \quad (9)$$

Its projection onto an arbitrary orbital ϕ_a orthogonal to all current orbitals is

$$\left\langle \phi_a \left| \frac{\partial L}{\partial \phi_m^*} \right. \right\rangle \stackrel{\text{SD}}{=} 2 f_a^m, \quad (10)$$

vanishing of which with the optimal orbitals is the Brillouin condition.

For multiconfigurational states Eqs. (3) and (6) for the Lagrangian gradient and multipliers take the SD-like form when the 2-RDM is rewritten in terms of its cumulant (see Appendix A). This nominally results in replacements $h \rightarrow f$, $\gamma \rightarrow \lambda$:

$$\left| \frac{\partial L}{\partial \phi_m^*} \right\rangle = 2 \left(\gamma_i^m \hat{f} + \lambda_{ij}^{mk} \hat{g}_k^{ij} - \epsilon_i^m \right) |\phi_i\rangle, \quad (11)$$

$$\epsilon_n^m = \gamma_i^m f_n^i + \lambda_{ij}^{mk} g_{nk}^{ij}. \quad (12)$$

Clearly, Eq. (9) follows from Eq. (11) due to the vanishing 2-RDM cumulant for the SD state.

Note that the single determinant expression for the gradient with respect to orbital ϕ_m (Eq. (9)) only involves the action of the Fock operator onto ϕ_m itself. In contrast, the $\gamma_i^m \hat{f} |\phi_i\rangle$ contribution to the multideterminantal expression (15) involves the action of the Fock operator on *every* orbital. The use of *natural* orbitals (NOs), which make the 1-RDM diagonal,

$$\gamma_n^m \stackrel{\text{NO}}{=} \begin{cases} \gamma_m^m, & m = n \\ 0, & m \neq n \end{cases} \quad (13)$$

allows to eliminate the *kinematic* coupling between the gradients:

$$\left\langle \frac{\partial L}{\partial \phi_m^*} \right\rangle \stackrel{\text{NO}}{=} 2 \left(\gamma_m^m \hat{f} |\phi_m\rangle + (\lambda_{ij}^{mk} \hat{g}_k^j - \epsilon_i^m) |\phi_i\rangle \right). \quad (14)$$

Until now the formalism has been completely generic, i.e., applicable to any real-space representation. However, the manner in which Eq. (4) must be solved differs between numerical representation. Thus it is now necessary to specialize the formalism to the MRA numerical representation used in this work that we introduced in Section 1. Orbital optimization in the MRA representation in both SD²³ and correlated⁵² contexts uses the integral reformulation of the differential equations (this is crucial for being able to solve differential equations in *discontinuous* spectral element basis). Partitioning the Fock operator \hat{f} into the free-particle Hamiltonian \hat{d} and potential \hat{v} (see Eq. (33)), the orbital stationarity condition becomes:

$$-\left(\hat{d} - \tilde{\epsilon}_m\right) |\phi_m\rangle = \hat{v} |\phi_m\rangle + \frac{1}{\gamma_m^m} \left(\gamma_{ij}^{mk} \hat{g}_k^j |\phi_i\rangle - \sum_{i \neq m} \epsilon_i^m |\phi_i\rangle \right), \quad (15)$$

where

$$\tilde{\epsilon}_m \equiv \frac{\epsilon_m^m}{\gamma_m^m} \stackrel{\text{NO}}{=} f_m^m + \sum_{ijk} \frac{\lambda_{ij}^{mk} g_{mk}^{ij}}{\gamma_m^m} = h_m^m + \sum_{ijk} \frac{\gamma_{ij}^{mk} g_{mk}^{ij}}{\gamma_m^m} \quad (16)$$

is the effective energy of NO m . Note that the natural orbital basis is essential for the integral reformulation since it eliminates all but a single instance of the differential operator \hat{d} ; solving for the natural orbitals is thus most sound strategy in the MRA numerical representation!

The orbital update described below exploits the fact that $\tilde{\epsilon}_m < 0$ for all orbitals, even weakly occupied. This may appear counterintuitive, since we normally think of unoccupied orbitals as corresponding to positive energies. To rationalize this observation, consider decomposition of the electronic energy, Eq. (1), into the contributions from natural orbital m and the rest:

$$\begin{aligned} E &\equiv E_m + E_{-m} \\ E_m &\equiv 2 \operatorname{Re} \left(\gamma_m^m h_m^m + \sum_{ijk} \gamma_{ij}^{km} g_{km}^{ij} \right) = 2 \operatorname{Re} \epsilon_m^m. \end{aligned} \quad (17)$$

Since the electronic energy becomes more negative as the orbital basis is expanded, E_m approximates the absolute *decrease* in the energy due to the addition of orbital m to the orbital set. A more rigorous mathematical analysis may be warranted, but the simple argument should suffice for now.

Updated orbitals are obtained by the action of Green's operator of particle in constant potential $-\tilde{\epsilon}_m > 0$ on the r.h.s. of Eq. (15):

$$|\phi_m\rangle = -\hat{G}_{-\tilde{\epsilon}_m} \left(\hat{v} |\phi_m\rangle + \frac{1}{\gamma_m^m} \left(\lambda_{ij}^{mk} \hat{g}_k^j |\phi_i\rangle - \sum_{i \neq m} \epsilon_i^m |\phi_i\rangle \right) \right). \quad (18)$$

For a nonrelativistic particle and open boundary conditions Green's operator has the familiar

Yukawa kernel:

$$x > 0 : \hat{G}_{-x}f(\mathbf{r}) = -2 \int \frac{\exp(-\sqrt{2x}|\mathbf{r} - \mathbf{r}'|)}{4\pi|\mathbf{r} - \mathbf{r}'|} f(\mathbf{r}') d\mathbf{r}' \quad (19)$$

extensions to the periodic boundary conditions⁶⁵ and Dirac particles⁶⁶ are also known. The updated orbitals are not orthonormal, thus the standard symmetric (Löwdin) orthonormalization⁶⁷ is applied to restore the orbital orthonormality while minimizing the induced change to facilitate extrapolation.⁶⁸

For highly-symmetric cases, like NOs with high angular momentum in atoms, it may be also desirable to project orbitals onto the corresponding invariant subspaces of the symmetry group. This is due to the spectral element basis lacking the desired symmetry properties, thus symmetries of the orbitals are maintained to precision ϵ used to define the basis; this is further compounded by the additional approximations invoked when evaluating Eq. (18). Appendix B described the relevant projection scheme used for the case of atoms where the problem can become particularly severe when low precision ($\epsilon > 10^{-4}$) is used.

The rate of convergence of Eq. (18) is rapid, but it is possible to accelerate it further by extrapolation. To this end we deploy the Krylov-subspace Accelerated Inexact Newton (KAIN) method;⁶⁹ other strategies like the Broyden–Fletcher–Goldfarb–Shanno (BFGS) method⁷⁰ should be usable as well. Note that to be able to make KAIN extrapolation robust it is essential to choose a canonical frame for the orbitals. Detailed description of the canonicalization approach are outside of the scope of this article (canonicalization is only essential for accelerating the solver) and will be reported elsewhere.

It is useful to point out how Eq. (18) is related to the orbital update used to determine optimal single-determinant (SD) orbitals in Ref. 23. For a single determinant the cumulant

vanishes,

$$\epsilon_n^m \stackrel{\text{SD}}{=} f_n^m, \quad \text{and} \tag{20}$$

$$\gamma_n^m \stackrel{\text{SD}}{=} \delta_n^m; \tag{21}$$

hence the orbitals are automatically natural and the gradients (9) are kinematically decoupled. The residual coupling in the SD version of (18) is via the Lagrange multipliers. Such coupling can be removed completely by switching to the *canonical* orbitals which make the Fock operator diagonal ($f_n^m = \delta_n^m \epsilon_m$) and simplify the orbital update to

$$|\phi_m\rangle \stackrel{\text{SD}}{=} -\hat{G}_{-\epsilon_m} \hat{v} |\phi_m\rangle. \tag{22}$$

This coincides with the standard orbital update used for single determinant SCF solver in **MADNESS** when orbitals are not localized; with localized orbitals the SD version of Eq. (18) (with all cumulant contributions omitted) is used instead. Note that in all of these approaches the Lagrange multipliers are evaluated every iteration directly (as matrix elements of the Fock operator in the basis of current orbitals) rather than iteratively updated as in the original solver described in Ref. 23.

Specialization of Eqs. (12) and (18) for the important case of the complete active space is straightforward, namely for inactive orbitals the cumulant contributions vanish. No additional changes are needed.

3 Technical Details

The orbital solver has been implemented in a developmental version of the Massively Parallel Quantum Chemistry (MPQC) package⁷¹ using the implementation of the MRA calculus in the **MADNESS** library.⁶³ The solver is bootstrapped with Gaussian AOs taken from the user-provided basis and projected onto the spectral element basis. Mean-field orbitals are then

obtained by optimization within the projected AO basis. RDMs were obtained from 1- and 2-electron integrals evaluated in the mean-field (SCF) orbitals expressed in real-space basis using a Heat-Bath CI (HCI)⁷² solver developed in MPQC. All computations on atoms and the minimal-basis H₁₀ computation set HCI selection thresholds $\epsilon_{1,2}$ to zero; the H₁₀ computation bootstrapped from the cc-pV{D,T}Z bases used $\epsilon_{\{1,2\}} = 10^{\{-4,-6\}}$.

4 Results

4.1 Atoms

4.1.1 He

The CI energies obtained with fixed Gaussian AO bases and the corresponding spectral-element orbitals obtained therefrom are shown in Table 1.

Unsurprisingly, the use of optimized numerical orbitals results in significant lowerings of the CI energy. Clearly, orbital optimization alone only addresses the suboptimality of the given orbital set of a fixed finite rank (“orbital error”, quantified by $E_{\text{AO}} - E_{\text{MRA}}$); the basis set incompleteness due to the finite rank (“rank error”, quantified by $E_{\text{MRA}} - E_{\text{exact}}$) is not addressed by the orbital optimization and requires increasing the rank (ideally, in conjunction with extrapolation or explicit correlation). Nevertheless, it is somewhat surprising how substantial is the the orbital errors of the correlation consistent basis sets (that are optimized for atomic CI energies) relative to their rank errors, shown in the second-to-last column in Table 1. Even for a quadruple-zeta basis orbital relaxation lowers the energy by 60% of the residual basis set error. These findings are in line with the unexpected sensitivity of the CC singles and doubles energy to the details of the unoccupied (pair-natural) orbitals that we found in the LCAO context.⁷³

What is more surprising, however, is that usually significant (> 50%) fraction of the energy lowering due to the orbital optimization can be attributed to the relaxation of the

weakly-occupied (correlating) orbitals. To estimate this fraction the last column shows the the energy lowering due to relaxing the occupied Hartree-Fock (1s) orbital from its finite basis form to the exact form, as a percentage of the total CI energy lowering due to the orbital optimization. For example, with the cc-pVTZ AO basis only 33 % of the CI energy lowering can be attributed to the basis set incompleteness of the Hartree-Fock occupied orbital; this is somewhat unexpected considering that the correlation consistent basis family was optimized for atomic CI computations. This finding emphasizes that even numerical deficiencies of even weakly occupied orbitals can contribute significantly to the overall basis set errors of correlated energies.

Table 1: Converged CI energies (mE_h) of the ground-state He atom evaluated with fixed Gaussian AO and optimized MRA orbitals. The exact energy is $-2903.724 mE_h$. The energies are converged to all digits shown.

Basis ^a	AO		MRA		AO vs MRA	
	E_{AO}	$E_{AO} - E_{\text{exact}}$	E_{MRA}	$E_{MRA} - E_{\text{exact}}$	$\frac{E_{AO} - E_{MRA}}{E_{MRA} - E_{\text{exact}}} \times 100\%$	$\frac{E_{AO}^{\text{HF}} - E_{\text{exact}}^{\text{HF}}}{E_{AO} - E_{MRA}} \times 100\%$
1s	-2 846.292	57.43	-2 861.679	42.05	37	100
2s1p	-2 887.595	16.13	-2 897.674	6.05	167	64
3s2p1d	-2 900.232	3.49	-2 901.840	1.88	86	33
4s3p2d1f	-2 902.411	1.31	-2 902.909	0.82	61	34
5s4p3d2f1g	-2 903.152	0.57	-2 903.297	0.43	35	40

^a Gaussian computations used the standard STO-6G^{74,75} and cc-pV{D,T,Q,5}Z⁷⁶ basis sets, respectively.

MRA orbitals were obtained by optimization starting from the Gaussian AO basis sets.

As Figure 1 illustrates, the changes in the natural orbitals due to the basis set relaxation can indeed be significant, not only near the nucleus (where Gaussian orbitals lack the cusp) and far from the nucleus (where Gaussians decay too quickly) but also at the intermediate distances from the nucleus where the orbital magnitude and positions of the radial nodes can be strongly impacted by the orbital optimization.

As illustrated in Table 2, the orbital solver can robustly optimize orbital sets with occupancies differing by many orders of magnitude. As elaborated in Section 2, the effective orbital energy, $\tilde{\epsilon}$, that controls the orbital update via the Green’s operator (Eq. (18)) is negative even for the weakly-occupied NOs; in fact, they are even more negative than the energy of the strongly occupied NO. In contrast, the corresponding diagonal elements of

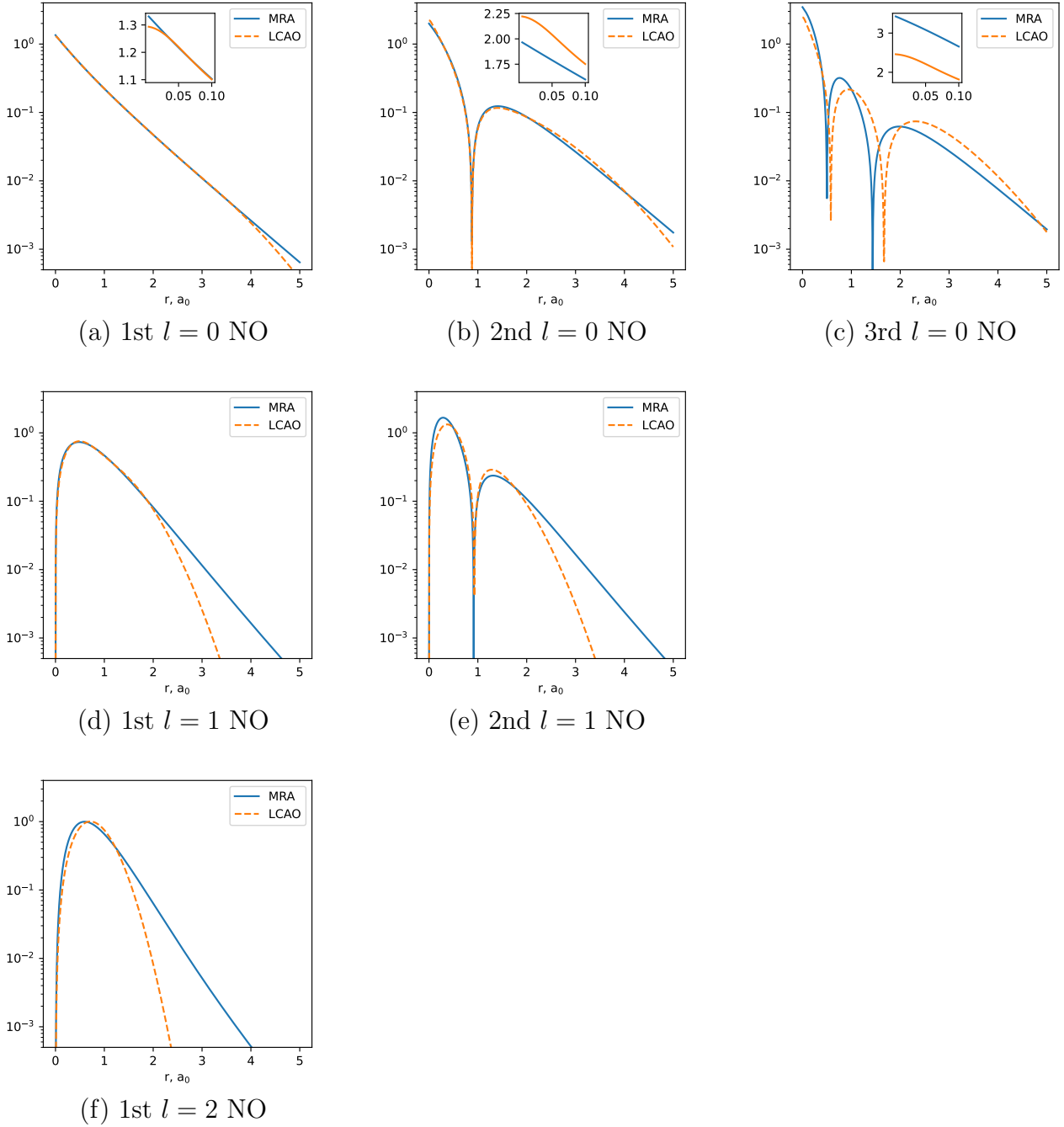


Figure 1: Comparison of 6 largest-occupancy NOs of the ground-state He atom evaluated using Gaussian cc-pVTZ basis (“LCAO”) and the real-space orbitals (“MRA”) obtained therefrom. Gaussian-based NOs decay too rapidly in the asymptotic limit as well as fail to reproduce the cusp at the nucleus for the $l = 0$ case.

the Fock operator are positive, as expected. The difference between the Fock and effective orbital energies is negligible for the strongly occupied NO.

Table 2: Properties of the leading natural orbitals for the He ground state obtained from the cc-pVTZ basis.

ϕ_p	γ_p^p	F_p^p, E_h	$\tilde{\epsilon}_p^p, E_h$
1s	1.984	-0.913	-0.958
2s	7.69×10^{-3}	1.595	-2.935
2p	2.60×10^{-3}	2.058	-3.305
3s	1.08×10^{-4}	7.400	-8.319
3p	7.05×10^{-5}	7.879	-8.789
3d	5.85×10^{-5}	5.927	-6.997

4.1.2 Be

For the ground state of Be the energy lowering due to the orbital relaxation was similar to what was found for He (see Table Table 3. Microhartree-level agreement was found with the atomic CI solver in the state-of-the-art GRASP2K package.⁷⁷

Table 3: CI energies (mE_h) of the ground-state Be atom evaluated with fixed pre-optimized Gaussian AOs (“LCAO”) and the matching numerical orbitals optimized using the approach described in this work (“MRA”) and the standard atomic finite-difference MCSCF solver in the GRASP2K software (“FD”).⁷⁷

Basis ^a	LCAO	MRA	FD
2s1p	-14.556 089	-14.616 856	-14.616 854
3s2p1d	-14.617 410	-14.654 415	-14.654 406
4s3p2d1f	-14.623 808	-14.661 475	-14.661 478
complete	-14.667 354 7 ^b		

^a Gaussian computations used the standard cc-pV{D,T,Q}Z⁷⁸ basis sets, respectively. MRA orbitals were obtained by optimization starting from the Gaussian AO basis sets.

^b Ref. 79.

4.2 Molecules

4.2.1 Bond breaking in HF and H₂O

Valence CASSCF computations on the standard small-molecule benchmarks (hydrogen fluoride, water) were performed to illustrate the robustness of the real-space solver for computation on general (nonlinear) molecules with varying character of electron correlation. Namely, CASSCF energy were determined with bond distances stretched from its equilibrium value

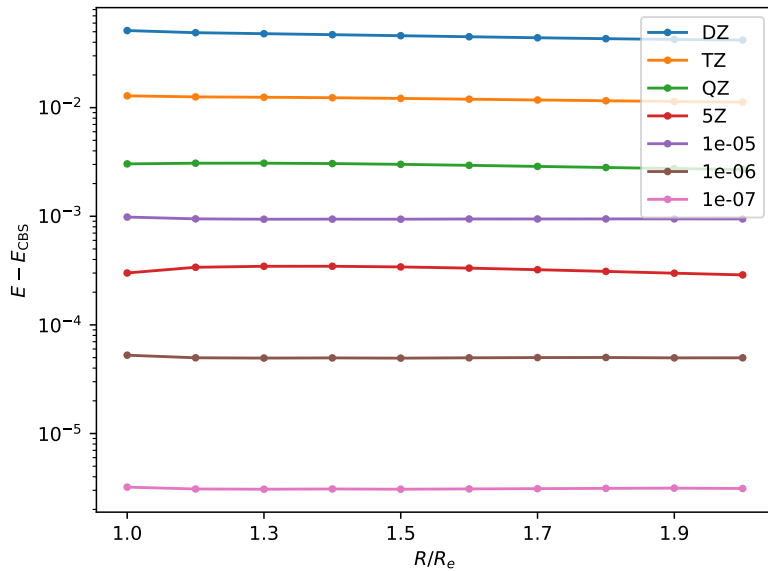
($R_e = \{0.9168, 0.9572\} \text{Å}$ for HF and H₂O, respectively) to twice the equilibrium value; the 104.52 degree bond angle in the latter was kept constant.

Figure 2 illustrates the basis set errors as a function of the bond distance for Gaussian AO CASSCF energies (obtained using the open-source BAGEL package⁸⁰ with the cc-pVXZ-JKFIT density fitting bases used to approximate the 2-electron integrals) as well as our MRA representation with varying precision ϵ . Already for $\epsilon = 10^{-5}$ the real-space representation is more accurate than the cc-pVQZ Gaussian basis. Further tightening of ϵ reduced the error below that of cc-pV5Z Gaussian result, with the most precise energies obtained with the MRA approach, $\epsilon = 10^{-8}$, likely converged to below a microhartree.

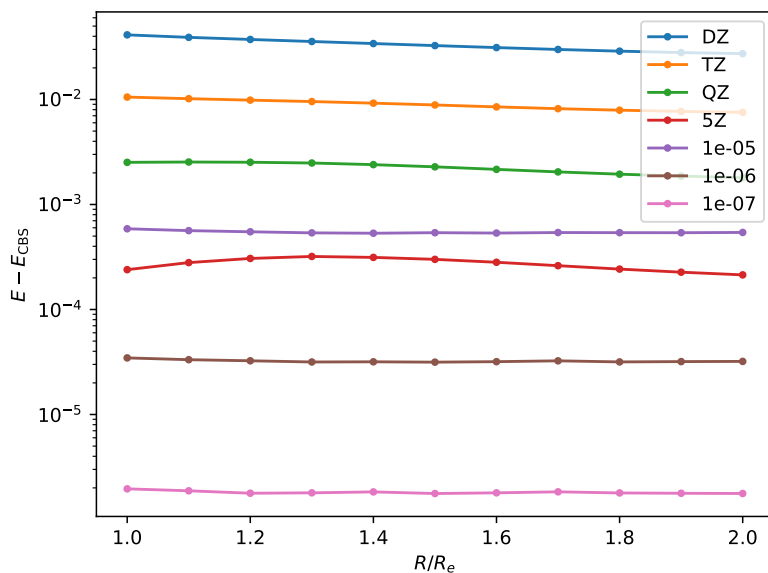
The logarithmic scale needed to illustrate the vast range of basis set errors ($> 20mE_h$ with the cc-pVDZ basis, few μE_h with MRA $\epsilon = 10^{-7}$) obscures the strong (and sometimes nonmonotonic) variation of basis set errors of the Gaussian AO representations. For example, the nonparallelity errors (defined as the largest minus the smallest error in the range) of the cc-pVDZ CASSCF energies are $\{9.4, 13.9\} mE_h$ for HF and H₂O, respectively, and are large fractions of the corresponding $\{51.3, 41.2\} mE_h$ maximum basis set errors. Importantly, the MRA energies have significantly smaller ratios of largest basis set errors to the nonparallelity errors than the Gaussian AO counterparts. For $\epsilon = 10^{-5}$ the nonparallelity errors are only $\{45, 54\} \mu E_h$ respectively, compared to the $\{984, 587\} \mu E_h$ largest basis set errors in the range; the corresponding values for the cc-pV5Z CASSCF are $\{58, 106\}$ and $\{347, 320\} \mu E_h$, respectively. The errors in MRA energies seem to cancel more systematically than the Gaussian AO counterparts, despite the intuition suggesting the latter should exhibit superior cancellation of errors.

4.2.2 H₁₀

We chose H₁₀ in its ground state as a model system for testing solver robustness due to the availability of extensive benchmarks for a number of methods.⁸² The system offers the ability to control the nature and strength of electron correlation by varying the interatomic distance



(a) HF



(b) H₂O

Figure 2: Basis set errors (E_h) of valence CASSCF energies obtained with Gaussian AO (cc-pVXZ bases⁸¹) and real-space orbital representations with varying precision parameter ϵ for single (a) and double (b) bond stretching. Complete basis set values were estimated by the real-space valence CASSCF energies obtained with $\epsilon = 10^{-8}$.

and the size of the orbital basis. In particular, at short interatomic distances (R) even the smallest nonminimal (double-zeta) Gaussian AO basis becomes nearly linearly dependent and accurate evaluation of the Hamiltonian and the method-specific iterative solvers can become untenable. At short R the importance of angular correlation greatly increases compared to the equilibrium and stretched R . Lastly, the use of a minimal AO basis (1 orbital per atom) maximizes the degree of “on-site” repulsion and increases the extent of longitudinal correlation.

The initial investigation of our orbital solver focused on the maximally-compressed geometry considered in Ref. 82, where achieving the basis set limit with the standard Gaussian basis sets is difficult due to the rapid onset of ill-conditioning, which recently motivated developments of mixed numerical representations marrying Gaussian AOs with real-space approaches.⁸³ As expected, the orbital optimization greatly reduces the basis set incompleteness of the CI energy, as can be seen in the rightmost column of Table 4, by $\times 3.4$ for the STO-6G basis and by $\times 7.4$ for the cc-pVDZ basis. The estimated residual basis set error with the MRA-optimized cc-pVDZ orbitals is $< 3mE_h$ / atom; this is already comparable to the $1mE_h$ uncertainty in the estimated nonrelativistic energy at this distance.⁸²

Figure 3 contains the plots of the frontier natural orbitals (counterparts of the HOMO and LUMO Hartree-Fock orbitals). The qualitative structures of the LCAO and real-space NOs are similar: both exhibit the same number of nodes and the same symmetry with respect to the inversion center. As expected, and just like in the atoms, the real-space NOs exhibit correct nuclear cusps and slower asymptotic decay into the vacuum. Interestingly, however, real-space NOs have lower probability densities at most nuclei than their Gaussian counterparts.

Table 4: HF and CI energies (mE_h) of the equidistant 10-atom chain of H atoms at compressed geometry (interatomic separation of 1 a.u.; see Ref. 82 for more details) evaluated with Gaussian AOs (“LCAO”) and optimized real-space orbitals (“MRA”; $\epsilon = 10^{-5}$, bootstrapped from the corresponding Gaussian AO basis), as well as the ratio of the respective basis set errors.

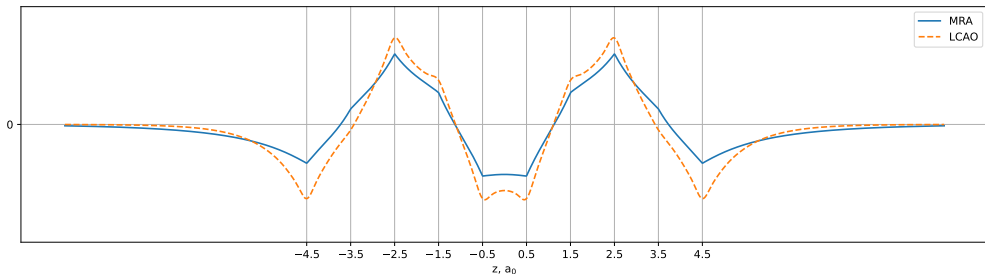
Basis ^a	HF		CI				
	LCAO		LCAO ^b		MRA	$\Delta_{\text{LCAO}}/\Delta_{\text{MRA}}$	
1s	-3,751.7	(406.3)	-3,824.4	(604.0)	-4,251.5	(176.9)	3.4
2s1p	-4,010.1	(147.9)	-4,219.7	(208.9)	-4,404.0	(24.4)	8.6
3s2p1d	-4,139.3	(18.7)	-4,394.5	(33.9)	-4,421.4	(7.0)	4.8
4s3p2d1f	-4,150.5	(7.5)	—	—	—	—	—
complete	-4,158.0		-4,428.4 ^c				

^a Gaussian computations used the standard STO-3G⁷⁴ and cc-pV{D,T,Q}Z⁸¹ basis sets.

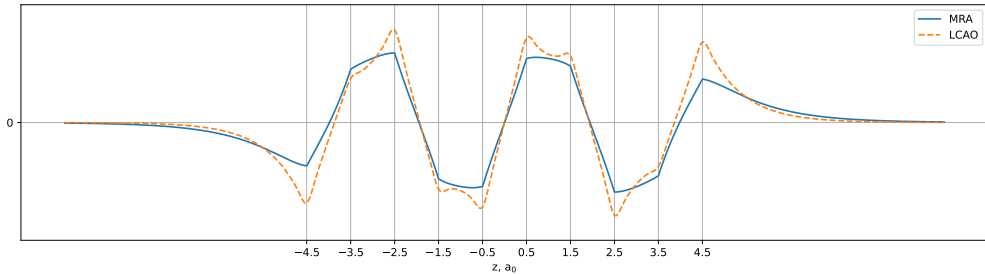
The MRA orbitals were obtained by optimization starting from the corresponding Gaussian AO basis sets.

^b The corresponding MRCI+Q values from Ref. 82 are -3,824.4 (STO-6G) and -4,219.5 (cc-pVDZ); MRCI did not converge with triple- and quadruple-zeta bases.

^c Estimated CBS auxiliary field quantum Monte Carlo (AFQMC) energy from Ref. 82.



(a) 5th NO



(b) 6th NO

Figure 3: Plots of frontier NOs of H_{10} evaluated with STO-6G Gaussian AOs (“LCAO”) and the corresponding optimized real-space orbitals (“MRA”) along the molecular axis.

5 Summary and Perspective

We presented a general method for constructing orbitals that are optimal for computing energies with correlated (many-body methods) in arbitrary molecules and with robust control of numerical errors. In this work we employed a multiresolution adaptive discontinuous spectral-element representation for the orbitals, but the presented method can be used with other real-space representations. Although utilized with the conventional and selected configuration interaction wave functions, the orbital solver can be used with arbitrary maps from orbitals to 1- and 2-particle reduced density matrices (e.g., tensor networks, stochastic methods, or quantum circuits). Numerical performance of the method was demonstrated by computing the CI energies of small atoms (matching the numerical precision of the atomic finite-difference CI codes) and a paradigmatic compressed polyatomic molecule; in all cases the use of real-space representation for the orbitals yielded energies that were significantly lower than the Gaussian AO-based counterparts, with correct asymptotic behavior at the nuclei and in vacuum.

Despite using the efficient production-grade implementation of the MRA calculus in `MADNESS`, the current implementation is not fully optimal. Although as we demonstrated here optimization of more than 100 *correlated* orbitals is already feasible with the current (CPU-only) code on a single multicore node, the implementation of the time-determining step in the orbital update, namely, the cumulant-dependent contribution to Eq. (18) (evaluated at the $\mathcal{O}(n_{\text{act}}^4)$ asymptotic cost, with n_{act} the number of active orbitals), does not explicitly optimize for CPU caches and can be significantly improved (by one to two orders of magnitude) even without exploiting accelerators. The optimization of 140 correlated orbitals in H_{10} reported in Section 4.2.2 took less than 4 hours per iteration on a single node of the `TinkerCliffs` cluster at Virginia Tech’s Advanced Research Computing equipped with a 128-core AMD EPYC 7702 processor; this was already comparable with 30 minutes per iteration that the selected CI 2-RDM evaluation took.

The implementation can also be improved in the other asymptotic regime, namely for

applications with a modest number of active orbitals ($n_a \leq 50$) and a large number of inactive orbitals, n_i . The asymptotic cost is then dominated by the evaluation of the exchange contribution to the $\hat{v}|\phi_m\rangle$ term on the right-hand side of Eq. (18). By orbital localization of the inactive orbitals fast application of the exchange operator will be possible, as demonstrated by the past development of the optimally-scaling MRA Hartree-Fock method.⁸⁴ In the current implementation the inactive orbitals are not localized, hence the cost of the exchange operator application is at worst $\mathcal{O}(n_c^3)$. Nevertheless practical applications to general systems can be readily performed without these optimizations. For example, a (4,4)-CASSCF($\epsilon = 10^{-5}$) evaluation of the ground state energy of the butadiene molecule took 380 seconds on an Apple MacBook Pro with a 12-core Apple M2 Max chip; for comparison, the state-of-the-art Hartree-Fock MRA solver in **MADNESS** took 130 seconds. We expect the described improvements to bring down the cost of the CAS computation with small active spaces close to the cost of the optimized MRA Hartree-Fock implementation. The conventional (4,4) CASSCF wave function of comparable quality requires a cc-pV5Z basis (see Table 5); such computation with **BAGEL**⁸⁰ (using the matching cc-pV5Z-JKFIT density fitting basis) on the same machine took 186 seconds.

Table 5: Basis set errors of the ground state (4,4) CASSCF energies evaluated in LCAO and MRA representations for the (1,3)-butadiene molecule at the experimentally-derived equilibrium geometry.⁸⁵

Basis ^a	δE^b
DZ	54.05
TZ	12.57
QZ	2.73
5Z	0.38
MRA($\epsilon = 10^{-5}$)	0.73
MRA($\epsilon = 10^{-6}$)	0.06

^a XZ denotes the cc-pVXZ Gaussian AO basis set.⁸¹

^b Error in mE_h relative to the MRA($\epsilon = 10^{-7}$) energy, $-155.041338 E_h$.

After the outlined algorithmic improvements we expect the cost of orbital optimization to become largely trivial relative to the wave function/density optimization. We are thus

hopeful that the real-space representations will become competitive with or even preferred to the AO representations for correlated models.

Our formalism should map straightforwardly to the optimization of molecular spinors for relativistic correlated methods by borrowing the advances in 4-component relativistic numerical electronic structure introduced by some of us recently.⁶⁶ Extension to periodic systems is also straightforward by using the existing extension of Poisson and Helmholtz Green’s operators to periodic boundary conditions.⁶⁵ Work along these lines is already underway and will be reported elsewhere.

Acknowledgement

This work was supported by the U.S. Department of Energy via award DE-SC0022327. We are grateful to Greg Beylkin for providing the quadratures described in Ref. 86. The authors acknowledge Advanced Research Computing at Virginia Tech (<https://arc.vt.edu/>) for providing computational resources and technical support that have contributed to the results reported within this paper.

Appendix A Notation and Standard Definitions

In this work we largely follow a covariant tensor notation of the many-body quantum chemistry.^{87,88} Einstein summation convention is implied, unless sums over any index are shown explicitly: namely, summation is implied over every symbol that appears once in a *contravariant* (upper, bra) position and once as in a *covariant* (lower, ket) position in a given tensor *product*, with the summation range defined by the symbol. Spin-orbital basis is assumed throughout the paper for simplicity (the actual implementation is spin-adapted).

2- and 1-RDMs for state $|\Psi\rangle$ are defined as:

$$\gamma_{kl}^{ij} \equiv \langle \Psi | \hat{a}^i \hat{a}^j \hat{a}_l \hat{a}_k | \Psi \rangle, \quad (23)$$

$$\gamma_j^i \equiv \langle \Psi | \hat{a}^i \hat{a}_j | \Psi \rangle \equiv \frac{2}{N-1} \sum_k \gamma_{ik}^{jk}, \quad (24)$$

with $\hat{a}^i \equiv \hat{a}_i^\dagger$ and \hat{a}_i the standard creators and annihilators, respectively. If $|\Psi\rangle$ is a multiterminantal/multiconfiguration (MC) state it is convenient to represent 2-RDM as

$$\gamma_{kl}^{ij} \equiv \gamma_k^i \gamma_l^j - \gamma_l^i \gamma_k^j + \lambda_{kl}^{ij}, \quad (25)$$

with λ_{kl}^{ij} the 2-RDM *cumulant*.⁸⁹

Matrix elements of one-, two-, and higher-body operators are denoted in tensor notation as follows:

$$\langle p | \hat{o}(1) | q \rangle \equiv \int \phi_p^*(1) \hat{o}(1) \phi_q(1) d1 \equiv o_p^q \quad (26)$$

$$\langle p_1 p_2 | \hat{o}(1, 2) | q_1 q_2 \rangle \equiv \int \phi_{p_1}^*(1) \phi_{p_2}^*(2) \hat{o}(1, 2) \phi_{q_1}(1) \phi_{q_2}(2) d1 d2 \equiv o_{p_1 p_2}^{q_1 q_2}, \text{ etc.} \quad (27)$$

It is also convenient to use the tensor notation for potentials generated by orbital products:

$$\hat{o}_{p_2}^{q_2} | \phi_{q_1} \rangle \equiv \left(\int \phi_{p_2}^*(2) \hat{o}(1, 2) \phi_{q_2}(2) d2 \right) \phi_{q_1}(1). \quad (28)$$

All many-body operators in this manuscript are particle-symmetric, i.e. $o(1, 2) = o(2, 1)$, hence $o_{q_1 q_2}^{p_1 p_2} = o_{q_2 q_1}^{p_2 p_1}$. Matrix elements of the core (1-particle) Hamiltonian $\hat{o}(1) \equiv \hat{h}(1)$, composed of the free-particle Hamiltonian \hat{d} and the Coulomb potential due to the nuclei \hat{v}_n , are denoted by h_q^p . The corresponding matrix elements of the Coulomb 2-body interaction, $o(1, 2) \equiv |\mathbf{r}_1 - \mathbf{r}_2|^{-1}$, are denoted by g_{rs}^{pq} . s_q^p denotes the orbital overlap $\langle \phi_p | \phi_q \rangle$. δ_q^p denotes

the Kronecker delta:

$$\delta_q^p = \begin{cases} 1, & p = q \\ 0, & p \neq q \end{cases} \quad (29)$$

The Fock operator has the usual definition:

$$\hat{f} \equiv \hat{h} + \hat{j} - \hat{k}. \quad (30)$$

$\hat{h} \equiv \hat{d} + \hat{v}_n$ is the 1-particle (core) Hamiltonian, composed of the free particle Hamiltonian \hat{d} (i.e., the kinetic energy in the nonrelativistic case, or the Dirac Hamiltonian in the relativistic case) and the Coulomb potential due to the nuclei \hat{v}_n . \hat{j} , and \hat{k} in Eq. (30) the Coulomb and exchange contributions, respectively:

$$\hat{j} \equiv V \times, \quad (31)$$

$$\hat{k} |\phi_p\rangle \equiv \gamma_n^m \hat{g}_m^p |\phi_n\rangle, \quad (32)$$

with V the Coulomb potential generated by the electron density $\rho(\mathbf{r})$. Key to the approach in this paper is the partitioning of the Fock operator into the free particle Hamiltonian \hat{d} and the potential $\hat{v} \equiv \hat{v}_n + \hat{j} - \hat{k}$:

$$\hat{f} = \hat{d} + \hat{v}. \quad (33)$$

Evaluation of the electron density from the orbitals,

$$\rho(\mathbf{r}) \equiv \langle \mathbf{r} | \phi_m \rangle \gamma_m^n \langle \phi_n | \mathbf{r} \rangle, \quad (34)$$

as well as evaluation of the Coulomb operator (Eq. (32)) is efficient in the *natural* basis which makes the 1-RDM diagonal. The matrix elements of the Fock operator thus take the

familiar form:

$$f_q^p \equiv h_q^p + (g_{qs}^{pr} - g_{sq}^{pr}) \gamma_r^s. \quad (35)$$

Appendix B Spherical projection of orbital updates

In atomic computations it is useful to be able to obtain solutions with specific target number of subshells, e.g. 3s2p1d for a second-row atom. In general such solutions are saddle points; tracking such saddle points can fail if the gradient does not preserve the relevant symmetries exactly. Unfortunately the finite-precision spectral element bases employed in this work do not preserve spherical symmetry. Thus we need to impose symmetry restrictions on the orbital updates; without such restrictions the solutions may break spherical symmetry.

Consider a subshell of $2l + 1$ “noisy” orbitals. To project out the components of the orbitals corresponding to other angular momenta we want to express each atomic orbital as a product of its radial component $f(r)$ times the angular factor, i.e. as

$$\phi_i(\mathbf{r}) \approx f(r) \sum_m^{2l+1} u_i^m Y_{lm}(\theta, \phi), \quad (36)$$

where the angular component is written as a unitary linear combination of spherical harmonics to support arbitrary orientation of each orbital. We determine $f(r)$ by minimizing the average deviation of the subshell orbitals:

$$\Delta \equiv \sum_i^{2l+1} \left\| \phi_i(\mathbf{r}) - f(r) \sum_m^{2l+1} u_i^m Y_{lm}(\theta, \phi) \right\|_2. \quad (37)$$

The gradient with respect to f is:

$$\begin{aligned}
\frac{\delta\Delta}{\delta f} &= 2 \sum_i^{2l+1} \left\langle \phi_i - f \sum_m^{2l+1} u_i^m Y_{lm} \left| \sum_{m'}^{2l+1} u_i^{m'} Y_{lm'} \right. \right\rangle \\
&= 2 \sum_{m'}^{2l+1} u_i^{m'} \sum_i^{2l+1} \langle \phi_i | Y_{lm'} \rangle - 2f \sum_i^{2l+1} \sum_m^{2l+1} u_m^i \sum_{m'}^{2l+1} u_i^{m'} \delta_m^m \\
&= 2 \sum_{m'}^{2l+1} u_i^{m'} \sum_i^{2l+1} \langle \phi_i | Y_{lm'} \rangle - (4l+2)f
\end{aligned} \tag{38}$$

This suggests the following formula for f for the given fixed coefficients u :

$$f = \frac{1}{2l+1} \sum_{m'}^{2l+1} u_i^{m'} \sum_i^{2l+1} \langle \phi_i | Y_{lm'} \rangle. \tag{39}$$

To determine nearly-optimal values of coefficients u for a given subshell orbital i we evaluate its overlaps with the spherical harmonics $S_{m,g}^{(i)} \equiv \langle \phi_i | Y_{lm} \rangle (r_g)$ on a uniform radial grid $\{r_g = g\delta_r, \forall g = 1..n_g\}$. Here we set the grid size n_g to 10 and the grid extent $\delta_g(n_g + 1)$ to $\sqrt{\frac{2\pi^2}{T_i}}$, which is the de Broglie wavelength of a free particle with kinetic energy $T_i \equiv \langle \phi_i | \hat{T} | \phi_i \rangle$. Note that these kinetic energies are available since detection of orbital subshells also used their kinetic energies. Coefficients $u_i^{m'}$ are given by the left-hand singular vector corresponding to the largest singular value of $(\mathbf{S}^{(i)})_{m,g} \equiv S_{m,g}$. Angular integration is performed via the lowest-order (72 points) rotationally invariant quadratures of Ahrens and Beylkin.⁸⁶

References

- (1) Roothaan, C. C. J. New Developments in Molecular Orbital Theory. *Rev. Mod. Phys.* **1951**, *23*, 69–89.
- (2) Boys, S. F. Electronic Wave Functions. I. A General Method of Calculation for the Stationary States of Any Molecular System. *Proc. R. Soc. Math. Phys. Eng. Sci.* **1950**, *200*, 542–554.

- (3) Zener, C. Analytic Atomic Wave Functions. *Phys. Rev.* **1930**, *36*, 51–56.
- (4) Slater, J. C. Atomic Shielding Constants. *Phys. Rev.* **1930**, *36*, 57–64.
- (5) Blum, V.; Gehrke, R.; Hanke, F.; Havu, P.; Havu, V.; Ren, X.; Reuter, K.; Scheffler, M. Ab Initio Molecular Simulations with Numeric Atom-Centered Orbitals. *Comput. Phys. Commun.* **2009**, *180*, 2175–2196.
- (6) Schäfer, T.; Ramberger, B.; Kresse, G. Quartic Scaling MP2 for Solids: A Highly Parallelized Algorithm in the Plane Wave Basis. *J. Chem. Phys.* **2017**, *146*, 104101.
- (7) Bylaska, E. J.; Song, D.; Bauman, N. P.; Kowalski, K.; Claudino, D.; Humble, T. S. Quantum Solvers for Plane-Wave Hamiltonians: Abridging Virtual Spaces Through the Optimization of Pairwise Correlations. *Front. Chem.* **2021**, *9*, 603019.
- (8) Kato, T. On the Eigenfunctions of Many-particle Systems in Quantum Mechanics. *Commun. Pure Appl. Math.* **1957**, *10*, 151–177.
- (9) Pack, R. T.; Byers Brown, W. Cusp Conditions for Molecular Wavefunctions. *J. Chem. Phys.* **1966**, *45*, 556.
- (10) Helgaker, T.; Klopper, W.; Koch, H. Basis-Set Convergence of Correlated Calculations on Water. *J. Chem. Phys.* **1997**, *106*, 9639–9646.
- (11) Klopper, W.; Manby, F. R.; Ten-no, S.; Valeev, E. F. R12 Methods in Explicitly Correlated Molecular Electronic Structure Theory. *Int. Rev. Phys. Chem.* **2006**, *25*, 427–468.
- (12) Kong, L.; Bischoff, F. A.; Valeev, E. F. Explicitly Correlated R12/F12 Methods for Electronic Structure. *Chem. Rev.* **2012**, *112*, 75–107.
- (13) Hättig, C.; Klopper, W.; Köhn, A.; Tew, D. P. Explicitly Correlated Electrons in Molecules. *Chem. Rev.* **2012**, *112*, 4–74.

- (14) Grüneis, A.; Shepherd, J. J.; Alavi, A.; Tew, D. P.; Booth, G. H. Explicitly Correlated Plane Waves: Accelerating Convergence in Periodic Wavefunction Expansions. *J. Chem. Phys.* **2013**, *139*, 084112.
- (15) Tajti, A.; Szalay, P. G.; Császár, A. G.; Kállay, M.; Gauss, J.; Valeev, E. F.; Flowers, B. A.; Vázquez, J.; Stanton, J. F. HEAT: High Accuracy Extrapolated Ab Initio Thermochemistry. *J. Chem. Phys.* **2004**, *121*, 11599–11613.
- (16) Barletta, P.; Shirin, S. V.; Zobov, N. F.; Polyansky, O. L.; Tennyson, J.; Valeev, E. F.; Császár, A. G. CVRQD Ab Initio Ground-State Adiabatic Potential Energy Surfaces for the Water Molecule. *J. Chem. Phys.* **2006**, *125*, 204307.
- (17) Pritchard, B. P.; Altarawy, D.; Didier, B.; Gibson, T. D.; Windus, T. L. New Basis Set Exchange: An Open, Up-to-Date Resource for the Molecular Sciences Community. *J. Chem. Inf. Model.* **2019**, *59*, 4814–4820.
- (18) VandeVondele, J.; Hutter, J. Gaussian Basis Sets for Accurate Calculations on Molecular Systems in Gas and Condensed Phases. *J. Chem. Phys.* **2007**, *127*, 114105.
- (19) Ye, H.-Z.; Berkelbach, T. C. Correlation-Consistent Gaussian Basis Sets for Solids Made Simple. *J. Chem. Theory Comput.* **2022**, *18*, 1595–1606.
- (20) Baranowska, A.; Sadlej, A. J. Polarized Basis Sets for Accurate Calculations of Static and Dynamic Electric Properties of Molecules. *J. Comput. Chem.* **2009**, NA–NA.
- (21) Chelikowsky, J. R.; Troullier, N.; Saad, Y. Finite-Difference-Pseudopotential Method: Electronic Structure Calculations without a Basis. *Phys. Rev. Lett.* **1994**, *72*, 1240–1243.
- (22) Briggs, E. L.; Sullivan, D. J.; Bernholc, J. Large-Scale Electronic-Structure Calculations with Multigrid Acceleration. *Phys. Rev. B* **1995**, *52*, R5471–R5474.

- (23) Harrison, R. J.; Fann, G. I.; Yanai, T.; Gan, Z.; Beylkin, G. Multiresolution Quantum Chemistry: Basic Theory and Initial Applications. *J. Chem. Phys.* **2004**, *121*, 11587–11598.
- (24) Fattebert, J. L.; Gygi, F. Linear-Scaling First-Principles Molecular Dynamics with Plane-Waves Accuracy. *Phys. Rev. B* **2006**, *73*, 489.
- (25) Genovese, L.; Neelov, A.; Goedecker, S.; Deutsch, T.; Ghasemi, S. A.; Willand, A.; Caliste, D.; Zilberberg, O.; Rayson, M.; Bergman, A.; Schneider, R. Daubechies Wavelets as a Basis Set for Density Functional Pseudopotential Calculations. *J. Chem. Phys.* **2008**, *129*, 014109.
- (26) Ohba, N.; Ogata, S.; Kouno, T.; Tamura, T.; Kobayashi, R. Linear Scaling Algorithm of Real-Space Density Functional Theory of Electrons with Correlated Overlapping Domains. *Computer Physics Communications* **2012**, *183*, 1664–1673.
- (27) Motamarri, P.; Nowak, M.; Leiter, K.; Knap, J.; Gavini, V. Higher-Order Adaptive Finite-Element Methods for Kohn–Sham Density Functional Theory. *J. Comp. Phys.* **2013**, *253*, 308–343.
- (28) Yanai, T.; Fann, G. I.; Beylkin, G.; Harrison, R. J. Multiresolution Quantum Chemistry in Multiwavelet Bases: Excited States from Time-Dependent Hartree–Fock and Density Functional Theory via Linear Response. *Phys. Chem. Chem. Phys.* **2015**, *17*, 31405–31416.
- (29) Jensen, S. R.; Flå, T.; Jonsson, D.; Monstad, R. S.; Ruud, K.; Frediani, L. Magnetic Properties with Multiwavelets and DFT: The Complete Basis Set Limit Achieved. *Phys. Chem. Chem. Phys.* **2016**, *18*, 21145–21161.
- (30) Xu, Q.; Wang, S.; Xue, L.; Shao, X.; Gao, P.; Lv, J.; Wang, Y.; Ma, Y. *Ab Initio* Electronic Structure Calculations Using a Real-Space Chebyshev-filtered Subspace Iteration Method. *J. Phys.: Condens. Matter* **2019**, *31*, 455901.

- (31) Jeziorski, B.; Monkhorst, H. J.; Szalewicz, K.; Zabolitzky, J. G. Atomic and Molecular Correlation Energies with Explicitly Correlated Gaussian Geminals. III. Coupled Cluster Treatment for He, Be, H₂, and LiH. *J. Chem. Phys.* **1984**, *81*, 368–388.
- (32) Flores, J. R. High Precision Atomic Computations from Finite Element Techniques: Second-order Correlation Energies of Rare Gas Atoms. *J. Chem. Phys.* **1993**, *98*, 5642–5647.
- (33) Ackermann, J. Finite-Element-Method Expectation Values for Correlated Two-Electron Wave Functions. *Phys. Rev. A* **1995**, *52*, 1968–1975.
- (34) Flores, J. R.; Kolb, D. Atomic MP2 Correlation Energies Fast and Accurately Calculated by FEM Extrapolations. *J. Phys. B At. Mol. Opt. Phys.* **1999**, *32*, 779.
- (35) Flores, J. R. New Benchmarks for the Second-Order Correlation Energies of Ne and Ar through the Finite Element MP2 Method: Second-Order Correlation Energies of Ne and Ar. *Int. J. Quantum Chem.* **2008**, *108*, 2172–2177.
- (36) Bischoff, F. A.; Harrison, R. J.; Valeev, E. F. Computing Many-Body Wave Functions with Guaranteed Precision: The First-Order Møller-Plesset Wave Function for the Ground State of Helium Atom. *J. Chem. Phys.* **2012**, *137*, 104103.
- (37) Bischoff, F. A.; Valeev, E. F. Computing Molecular Correlation Energies with Guaranteed Precision. *J. Chem. Phys.* **2013**, *139*, 114106.
- (38) Kottmann, J. S.; Bischoff, F. A. Coupled-Cluster in Real Space. 1. CC2 Ground State Energies Using Multiresolution Analysis. *J. Chem. Theory Comput.* **2017**, *13*, 5945–5955.
- (39) Kottmann, J. S.; Bischoff, F. A. Coupled-Cluster in Real Space. 2. CC2 Excited States Using Multiresolution Analysis. *J. Chem. Theory Comput.* **2017**, *13*, 5956–5965.

- (40) Wilson, S.; Silver, D. M. Algebraic Approximation in Many-Body Perturbation Theory. *Phys. Rev. A* **1976**, *14*, 1949–1960.
- (41) Fischer, C. F. Superposition of Configuration Results for SI II. *ApJ* **1968**, *151*, 759.
- (42) Fischer, C. F. Average-Energy-of-Configuration Hartree-Fock Results for the Atoms Helium to Radon Charlotte Froese Fischer. *Atomic Data and Nuclear Data Tables* **1972**, *4*, 301–399.
- (43) Sundholm, D.; Olsen, J.; Malmqvist, P.-Å.; Roos, B. O. In *Numerical Determination of the Electronic Structure of Atoms, Diatomic and Polyatomic Molecules*; De-
franceschi, M., Delhalle, J., Eds.; Springer Netherlands: Dordrecht, 1989; pp 329–334.
- (44) Johnson, W. R.; Sapirstein, J. Computation of Second-Order Many-Body Corrections in Relativistic Atomic Systems. *Phys. Rev. Lett.* **1986**, *57*, 1126–1129.
- (45) Dzuba, V. A.; Flambaum, V. V.; Kozlov, M. G. Combination of the Many-Body Perturbation Theory with the Configuration-Interaction Method. *Phys. Rev. A* **1996**, *54*, 3948–3959.
- (46) Adamowicz, L.; McCullough, E. A. A Numerical Multiconfiguration Self-consistent-field Method for Diatomic Molecules. *J. Chem. Phys.* **1981**, *75*, 2475–2476.
- (47) Laaksonen, L.; Sundholm, D.; Pyykkö, P. Two-Dimensional Fully Numerical MC SCF Calculations on H₂ and LiH: The Dipole Moment of LiH. *Chemical Physics Letters* **1984**, *105*, 573–576.
- (48) McCullough, E. A.; Morrison, J.; Richman, K. W. Numerical Perturbation Calculations for Diatomic Molecules. *Faraday Symp. Chem. Soc.* **1984**, *19*, 165.
- (49) Adamowicz, L.; Bartlett, R. J. Coupled Cluster Calculations with Numerical Orbitals for Excited States of Polar Anions. *J. Chem. Phys.* **1985**, *83*, 6268–6274.

- (50) Adamowicz, L.; Bartlett, R. J.; McCullough, E. A. Towards Numerical Solutions of the Schrödinger Equation for Diatomic Molecules. *Phys. Rev. Lett.* **1985**, *54*, 426–429.
- (51) Lehtola, S. A Review on Non-relativistic, Fully Numerical Electronic Structure Calculations on Atoms and Diatomic Molecules. *Int J Quantum Chem* **2019**, *119*.
- (52) Kottmann, J. S.; Bischoff, F. A.; Valeev, E. F. Direct Determination of Optimal Pair-Natural Orbitals in a Real-Space Representation: The Second-Order Moller–Plesset Energy. *J. Chem. Phys.* **2020**, *152*, 074105.
- (53) Edmiston, C.; Krauss, M. Configuration-Interaction Calculation of H₃ and H₂. *J. Chem. Phys.* **1965**, *42*, 1119–1120.
- (54) Meyer, W. Ionization Energies of Water from PNO-CI Calculations. *Int. J. Quantum Chem.* **1971**, *5*, 341–348.
- (55) Neese, F.; Hansen, A.; Liakos, D. G. Efficient and Accurate Approximations to the Local Coupled Cluster Singles Doubles Method Using a Truncated Pair Natural Orbital Basis. *J. Chem. Phys.* **2009**, *131*, 064103.
- (56) Alpert, B. K. Sparse Representation of Smooth Linear Operators. Ph.D. thesis, Yale University, 1990.
- (57) Beylkin, G.; Coifman, R.; Rokhlin, V. Fast Wavelet Transforms and Numerical Algorithms I. *Commun. Pure Appl. Math.* **1991**, *44*, 141–183.
- (58) Alpert, B. K. A Class of Bases in L^2 for the Sparse Representation of Integral Operators. *SIAM J. Math. Anal.* **1993**, *24*, 246–262.
- (59) Alpert, B.; Beylkin, G.; Gines, D.; Vozovoi, L. Adaptive Solution of Partial Differential Equations in Multiwavelet Bases. *Journal of Computational Physics* **2002**, *182*, 149–190.

- (60) Beylkin, G.; Cheruvu, V.; Perez, F. Fast Adaptive Algorithms in the Non-Standard Form for Multidimensional Problems. *Appl. Comput. Harmon. Anal.* **2008**, *24*, 354–377.
- (61) Yanai, T.; Fann, G. I.; Gan, Z.; Harrison, R. J.; Beylkin, G. Multiresolution Quantum Chemistry in Multiwavelet Bases: Analytic Derivatives for Hartree–Fock and Density Functional Theory. *J. Chem. Phys.* **2004**, *121*, 2866.
- (62) Bischoff, F. A. Analytic Second Nuclear Derivatives of Hartree-Fock and DFT Using Multi-Resolution Analysis. *J. Chem. Phys.* **2017**, *146*, 124126.
- (63) Harrison, R. J. et al. MADNESS: A Multiresolution, Adaptive Numerical Environment for Scientific Simulation. *SIAM J. Sci. Comput.* **2016**, *38*, S123–S142.
- (64) Bischoff, F. A.; Valeev, E. F. Low-Order Tensor Approximations for Electronic Wave Functions: Hartree-Fock Method with Guaranteed Precision. *J. Chem. Phys.* **2011**, *134*, 104104.
- (65) Jia, J.; Hill, J. C.; Beylkin, G.; Harrison, R. J. MULTIREOLUTION FAST METHODS FOR A PERIODIC 3-D NAVIER-STOKES SOLVER. Proc. 8th Int. Symp. Distrib. Comput. Appl. Bus. Eng. Sci. 2009; pp 13–16.
- (66) Anderson, J.; Sundahl, B.; Harrison, R.; Beylkin, G. Dirac-Fock Calculations on Molecules in an Adaptive Multiwavelet Basis. *J. Chem. Phys.* **2019**, *151*, 234112.
- (67) Löwdin, P.-O. On the Non-Orthogonality Problem Connected with the Use of Atomic Wave Functions in the Theory of Molecules and Crystals. *J. Chem. Phys.* **1950**, *18*, 365–375.
- (68) Mayer, I. On Löwdin’s Method of Symmetric Orthogonalization*: Löwdin’s Method of Symmetric Orthogonalization. *Int. J. Quantum Chem.* **2002**, *90*, 63–65.

- (69) Harrison, R. J. Krylov Subspace Accelerated Inexact Newton Method for Linear and Nonlinear Equations. *J. Comput. Chem.* **2004**, *25*, 328–334.
- (70) Yao, Y.; Umrigar, C. J. Orbital Optimization in Selected Configuration Interaction Methods. *J. Chem. Theory Comput.* **2021**, *17*, 4183–4194.
- (71) Peng, C.; Lewis, C. A.; Wang, X.; Clement, M. C.; Pierce, K.; Rishi, V.; Pavošević, F.; Slattery, S.; Zhang, J.; Teke, N.; Kumar, A.; Masteran, C.; Asadchev, A.; Calvin, J. A.; Valeev, E. F. Massively Parallel Quantum Chemistry: A High-Performance Research Platform for Electronic Structure. *J. Chem. Phys.* **2020**, *153*, 044120.
- (72) Holmes, A. A.; Tubman, N. M.; Umrigar, C. J. Heat-Bath Configuration Interaction: An Efficient Selected Configuration Interaction Algorithm Inspired by Heat-Bath Sampling. *J. Chem. Theory Comput.* **2016**, *12*, 3674–3680.
- (73) Clement, M. C.; Zhang, J.; Lewis, C. A.; Yang, C.; Valeev, E. F. Optimized Pair Natural Orbitals for the Coupled Cluster Methods. *J. Chem. Theory Comput.* **2018**, *14*, 4581–4589.
- (74) Hehre, W. J. Self-Consistent Molecular-Orbital Methods. I. Use of Gaussian Expansions of Slater-Type Atomic Orbitals. *J. Chem. Phys.* **1969**, *51*, 2657.
- (75) Hehre, W. J.; Ditchfield, R.; Stewart, R. F.; Pople, J. A. Self-Consistent Molecular Orbital Methods. IV. Use of Gaussian Expansions of Slater-Type Orbitals. Extension to Second-Row Molecules. *J. Chem. Phys.* **1970**, *52*, 2769–2773.
- (76) Woon, D. E.; Dunning, T. H. Gaussian Basis Sets for Use in Correlated Molecular Calculations. IV. Calculation of Static Electrical Response Properties. *J. Chem. Phys.* **1994**, *100*, 2975–2988.
- (77) Jönsson, P.; Gaigalas, G.; Bieroń, J.; Fischer, C. F.; Grant, I. New Version: Grasp2K

- Relativistic Atomic Structure Package. *Computer Physics Communications* **2013**, *184*, 2197–2203.
- (78) Prascher, B. P.; Woon, D. E.; Peterson, K. A.; Dunning, T. H.; Wilson, A. K. Gaussian Basis Sets for Use in Correlated Molecular Calculations. VII. Valence, Core-Valence, and Scalar Relativistic Basis Sets for Li, Be, Na, and Mg. *Theor Chem Acc* **2011**, *128*, 69–82.
- (79) Sims, J. S.; Hagstrom, S. A. Hylleraas-Configuration-Interaction Study of the 1 S Ground State of Neutral Beryllium. *Phys. Rev. A* **2011**, *83*, 032518.
- (80) Shiozaki, T. BAGEL: Brilliantly Advanced General Electronic-structure Library. *WIREs Comput Mol Sci* **2018**, *8*.
- (81) Dunning, T. H. Gaussian Basis Sets for Use in Correlated Molecular Calculations. I. The Atoms Boron through Neon and Hydrogen. *J. Chem. Phys.* **1989**, *90*, 1007–1023.
- (82) Motta, M. et al. Towards the Solution of the Many-Electron Problem in Real Materials: Equation of State of the Hydrogen Chain with State-of-the-Art Many-Body Methods. *Phys. Rev. X* **2017**, *7*, 1.
- (83) Stoudenmire, E. M.; White, S. R. Sliced Basis Density Matrix Renormalization Group for Electronic Structure. *Phys. Rev. Lett.* **2017**, *119*, 046401.
- (84) Yanai, T.; Fann, G. I.; Gan, Z.; Harrison, R. J.; Beylkin, G. Multiresolution Quantum Chemistry in Multiwavelet Bases: Hartree–Fock Exchange. *J. Chem. Phys.* **2004**, *121*, 6680.
- (85) Haugen, W.; Trætteberg, M.; Kaufmann, F.; Motzfeldt, K.; Williams, D. H.; Bunnberg, E.; Djerassi, C.; Records, R. The Molecular Structure of 1,3-Butadiene and 1,3,5-Trans-Hexatriene. *Acta Chem. Scand.* **1966**, *20*, 1726–1728.

- (86) Ahrens, C.; Beylkin, G. Rotationally Invariant Quadratures for the Sphere. *Proc. R. Soc. A* **2009**, *465*, 3103–3125.
- (87) Harris, F. E.; Jeziorski, B.; Monkhorst, H. J. Contraction Theorem for the Algebraic Reduction of (Anti)Commutators Involving Operator Strings. *Phys. Rev. A* **1981**, *23*, 1632–1638.
- (88) Kutzelnigg, W. Quantum Chemistry in Fock Space. I. The Universal Wave and Energy Operators. *J. Chem. Phys.* **1982**, *77*, 3081–3097.
- (89) Kutzelnigg, W.; Mukherjee, D. Cumulant Expansion of the Reduced Density Matrices. *J. Chem. Phys.* **1999**, *110*, 2800–2809.

optimal orbitals for correlated Ψ

$$\frac{\partial \langle \Psi | e^{\hat{\kappa} - \hat{\kappa}^\dagger} \hat{H} e^{\hat{\kappa}^\dagger - \hat{\kappa}} | \Psi \rangle}{\partial \hat{\kappa}} = 0$$

adaptive multiresolution basis

